Practical method for the design of pretensioned fully grouted rockbolts in tunnels

A practical method for the design of pre-tensioned fully grouted rockbolts in tunnels

Masoud Ranjbarnia [1], Ahmad Fahimifar [2], Pierpaolo Oreste [3]

Abstract

This paper develops an analytical approach to quantitatively model the efficiency of the pre-tensioning of grouted rockbolts in terms of reduction of tunnel convergence. In this study, the distribution of force along the pre-tensioned fully grouted bolt is calculated by the assumption of a rigid connection between the bolt and the rock mass. A compressive force is then applied to the bolt head on tunnel surface to consider the shear relative displacement between the bolt and the rock mass. The magnitude of this compressive force is found by modeling of bolt boundaries stiffness.

Finally, the theoretical proposed approach is simplified to be used for the practical purposes. The results show if the stiff end plate is tightened to the bolt head (complete planner contact), the grouting effect of the pre-tensioned fully grouted bolts on tunnel stability can be neglected.

[1] PhD student, E-mail: m.ranjbarnia@aut.ac.ir. Department of Civil and Environmental Engineering, Amirkabir University of Technology (Tehran Polytechnic), Hafez Ave., Tehran, Iran

[2] Professor, Corresponding author, E-mail: fahim@aut.ac.ir. Department of Civil and Environmental Engineering, Amirkabir University of Technology (Tehran Polytechnic), Hafez Ave., Tehran, Iran

[3] Associate professor, E-mail: pierpaolo.oreste@polito.it. Department of Environmental, land and infrastructure Engineering, Politecnico di Torino, Corso Duca degli Abruzzi, 24 – 10129, Torino, Italy

Keywords: Analytical techniques; Tunneling; Pre-tensioning; Bolts

Introduction

The systematic grouted rockbolting is widely used as an effective technique in the design and construction of tunnels. The pre-tensioned rockbolts, which transfer initial compressive pressure to the rock mass in order to increase their performance and efficiency, are one of the best and the most appropriate supporting systems to be used in particular circumstances like delay in the bolt installation.

During last three decades, a great number of analytical methods have been developed for the study of passive grouted bolts in tunneling design. In a group of approaches, the obtaining of the engineering properties of reinforced rock mass has been focused e.g. with definition of a dimensionless parameter named as "*bolt density*" (which reflects the relative density of bolts with respect to the opening perimeter) to calculate the improved geo-mechanical properties of rock mass (Indraratna and Kaiser 1990a,b; Osguii and Oreste 2010), with introducing a dimensionless coefficient named as "*ground reinforcement- stiffness*" (the contrast of stiffnesses of ground and rockbolt) to be used as the multipliers to obtain the confinement stress of composite material (Carranza-Torres 2009), with presenting of a formulation for mechanical contribution of the rockbolts based on shear stress on the bolt surface (Bobet and Einstein 2011), with obtaining the elastic properties of the rock-bolt material using the shear-lag method (Bobet 2006), and with assuming the influence of bolting on rock mass as a pressure on the tunnel boundary (Bischoff and Smart 1975), as a fictitious increase of the rock mass cohesion (Grasso et al. 1989), and as an increase of confinement stress within rock mass (Fahimifar and Soroush 2005).

On the other hand, in another group of approaches, a comprehensive series of studies have been conducted by assuming that the grouted bolt contributes to rock mass in the form of a radial pressure within the influence zone of the rockbolt (Aydan 1989; Peila and Oreste 1995; Oreste and Peila 1996; Li and Stillborg 1999; Cai et al. 2004a, b; Guan et al. 2007; Bobet and Einstein 2011).

Unlike the passive grouted bolts, the study of pre-tensioned grouted bolts has not been of high interest so far, and their performance is still quantitatively unknown. A few attempts which were carried out were based on the development of the works originally performed for the passive reinforcements (Carranza-Torres 2009; Fahimifar and Ranjbarnia 2009; Bobet and Einstein 2011). Hence, they have involved great limitations which may cause them to give crude predictions.

In order to model the pre-tensioned grouted rockbolts as a systematic support of tunnels (at least for the short-time), the relation between the value of pre-tensioned pressure on the tunnel surface (produced by the pre-tensioned force) and that of the fictitious constrained radial pressure (supplied by the proximity of tunnel face) should be particularly taken into consideration. That is, the progressively advancing tunnel face in front of bolted section leads to diminishing of the fictitious constrained radial pressure to zero and ultimately, the pre-tensioned pressure will only remain. Provided that the value of pre-tensioned pressure on the tunnel surface is greater than the constrained radial pressure, advancement of the tunnel face will not change the stresses within the rock mass around tunnel, and the ultimate load will not be changed. Meanwhile, if the value of pre-tensioned pressure is less than the fictitious constrained radial pressure, the tunnel convergence will again occur immediately after the radial pressure becomes less than the initial value prior to bolt installation.

Remarking that above discussion is pertinent to the condition that tunnel convergence merely occurs due to tunnel face advancement (short-term movement).

Thus, the above-mentioned analytical approaches for the pre-tensioned grouted rockbolts are not appropriate solution due to either neglecting the relation of the pre-tensioned and the fictitious constrained pressures (Carranza-Torres 2009; Fahimifar and Ranjbarnia 2009) or considering constant bolt tensioning (Bobet and Einstein 2011).

In an effort to bridge this apparent gap in the available methods and tools for analysis of reinforced tunnel by the pre-tensioned grouted rockbolts, this paper develops an analytical approach to quantitatively model the efficiency of the pre-tensioning of grouted rockbolts in terms of reduction of both tunnel convergence.

The distribution of force along the bolt is an important issue. In general, the bolt axial force is originated by the relative shear displacements between the bolt and the rock mass which itself affected by both the shear stiffness and the bolt boundaries conditions. Some of the previously mentioned works have obtained the axial force along the bolt e.g. with modeling of shear stress between the bolt and the rock mass, and then integrating of the corresponding function (Li and Stillborg 1999), with considering the constitutive deformation between the bolt and rock mass, and taking derivation to obtain the differential equation of axial force (Cai et al. 2004a, b). In these efforts, the boundary conditions were not taken into account i.e. the force on the tunnel wall was considered zero. Meanwhile; by the in-situ measurements and the results of numerous numerical calculations, Oreste (2008) presented a simple two-line graphic for distribution of axial force along the bolt in which the force on tunnel wall is considered for the stiff end plate.

All these works have been carried out for the passive bolts while no attempt has been performed for the pre-tensioned grouted types. Hence, in this paper, a new methodology is also presented to compute the distribution of the force along the pre-tensioned grouted bolts. For this purpose, it is calculated by the assumption of a rigid connection between the bolt and the rock mass. A compressive force is then applied to the bolt head on tunnel surface (near boundary) to reduce the bolt force. The magnitude of this compressive force is dependent upon the near boundary condition (i.e. the stiffness of components of nut, washer, and the plate) and the far boundary condition of bolt (i.e. the shear stiffness of the initial anchored length). Therefore, these two boundaries conditions will be also modeled.

Finally, as the derived formula of the proposed model is too complicated for practice and preliminary design, a simple method will be introduced with employing the support and the rock mass interaction concepts on the basis of the proposed model.

Modeling of systematic pre-tensioned fully grouted bolts behavior in tunnels

General assumptions

A circular tunnel of radius r_i , under plane strain condition, is driven in a homogeneous, isotropic, initially elastic rock mass with a strain-softening behavior subjected to a hydrostatic stress field, p_0.

The problem is modeled with the assumption that tunnel closure is only occurred due to advancement of the tunnel face (which is equivalent to the reduction of fictitious radial pressure). Therefore, time-dependent properties of the rock mass are ignored, and short-term convergence of tunnel is only taken into account.

As the rockbolts are installed, a certain convergence of tunnel has already been occurred, and an initial plastic zone of radius $\bar{r}_e$ has been developed around the tunnel (Fig. 1a).

Theoretical concept of the pre-tensioned grouted rockbolts behavior in tunnel

The installation process of the pre-tensioned grouted rockbolt, in this paper, consists of placing a grouted anchor, tensioning the rockbolt and tying end of the bolt by nut and plate to the tunnel surface, and then grouting the remained of the bolt length. Once the pre-tensioned force is applied by the plate to tunnel surface, a radial pressure develops within the rock in the influence domain of itself. Therefore

$$p_{pre-ten} = \frac{T_{pre-ten}}{C_0} \tag{1}$$

where $T_{pre-ten}$ and $p_{pre-ten}$ are the pre-tensioned force and the associated radial pressure at tunnel surface, respectively. C_0 is the rockbolt effective area at tunnel surface calculated by

$$C_0 = S_l . S_{c_0} \tag{2}$$

S_l and S_{c_0} are the longitudinal and tangential space of bolts at tunnel surface, respectively.

The advancement of tunnel face is again restarted after full installation of bolts. Then, the remained fictitious radial pressure will be further reduced and will be ultimately diminished. Accordingly, two following different circumstances can occur:

***Case A*:** If the magnitude of the fictitious radial pressure is less than the radial pre-tensioned pressure, progressive advancement of tunnel face will not result in further radial displacement (Fig 1a). This is because, due to applying the pre-tensioned pressure, the remained radial pressure on tunnel surface (after full diminishing of the fictitious constrained pressure) is greater than the value prior to the bolt installation.

Thus, the final bolt force is not greater than the initial applied tension i.e. the bolt force will remain constant along the bolt and will equal to pre-tensioned force. As well, grouting the remained bolt length has no influence on its behavior mechanism but will protect the bolt from corrosion.

***Case B*:** If the magnitude of the fictitious constrained radial pressure is greater than the pre-tensioned pressure, somewhat re-advancing of tunnel face will lead to further inward radial displacement of the rock mass. So the bolt force will increase till to full diminishing of the fictitious constrained radial pressure, and the plastic radius will become greater (Fig. 1b).

Reminding that the magnitude of the pre-tensioned force is a significant fraction of the bolt's yielding capacity so that it does not have a final force to yield.

The analytical simulation of the radial pre-tensioned fully grouted bolts

Rigid (Ideal) connection between the bolt and rock mass

In general, the grouted rockbolts reinforce and mobilize the inherent strength of the rock mass by offering internal and confining pressure (Huang et al. 2002). Assuming that the bolt contribution is in the form of a radial load spread within its influencing zone, the differential equation of equilibrium for tunnel with circular cross section, uniform in-situ stresses, and close spacing of the rockbolts will be

$$\frac{d\sigma_r}{dr} = \frac{\sigma_\theta - \sigma_r}{r} + \frac{dT}{dr}\frac{r_i}{C_0}\frac{1}{r} \tag{3}$$

where σ_θ and σ_r are the tangential and radial stresses, respectively. r is a variable showing the radial distance from tunnel center, T is the overall rockbolt tensioned force.

For *Case A*, as discussed in section 2-2, tunnel convergence will not increase, and the force along the bolt will be almost constant and will equal to the pre-tensioned value i.e. $T = T_{pre-ten}$. Thus, dT/dr will be zero and Eq. (4) will be resulted from Eq. (3) (also by replacing of the Hoek- Brown strength criterion (1980) for rock mass)

$$\frac{d\sigma_r}{dr} = \frac{\left[m\sigma_c\sigma_r + s\sigma_c^2\right]^{1/2}}{r} \tag{4}$$

with the following boundary condition

(i) At $r = r_i$, $\sigma_r = p_i$ in which $p_{inst} \le p_i \le p_0$. (Because, $p_{pre-ten} > p_{inst}$)

(ii) At $r = r_e$, $\sigma_r = \sigma_{re}$.

where σ_c is uniaxial compressive strength of the intact rock material, and parameters m and s are rock mass constants depending on the nature of the rock mass and its geotechnical conditions. p_i is the magnitude of radial pressure in the tunnel surface, p_{inst} is the fictitious radial pressure induced by the working face at bolt installation time, and σ_{re} is the radial stress at the outer boundary of plastic zone and is obtained by (Hoek and Brown 1980)

$$\sigma_{re} = p_0 - M.\sigma_c \tag{5}$$

in which

$$M = \frac{1}{2}\left[\left(\frac{m_p}{4}\right)^2 + m_p\frac{p_0}{\sigma_c} + s_p\right]^{1/2} - \frac{m_p}{8} \tag{6}$$

where parameters m_p and s_p are rock mass constants before failure.

For *Case B*, dwindling of the radial pressure on tunnel surface from its remained value i.e. p_{inst} to pre-tensioned pressure i.e. $p_{pre-ten}$ leads to increase of radial deformations of rock mass, and imposes further tension to the bolt. Thus, the differential equation for this condition will be Eq. (3) with the following boundary conditions

(i) At $r = r_i$, $\sigma_r = p_i$ in which $p_{pre-ten} \le p_i \le p_{inst}$

(ii) At $r = r_e$, $\sigma_r = \sigma_{re}$

The bolt axial force can be obtained by

$$T = A_b . E_s . \varepsilon_b \tag{7}$$

where A_b and E_s are bolt cross section area and the modulus of elasticity of bolt, respectively, and ε_b is the bolt axial strain calculated by

$$\varepsilon_b = \varepsilon_r' + \varepsilon_{pre-ten} \tag{8}$$

where $\varepsilon_{pre-ten}$ is the pre-tensioned strain of rockbolts, and ε_r' is the radial strain within rock mass taking place after the bolts installation computed by

$$\varepsilon_r' = \begin{cases} \varepsilon_r - \bar{\varepsilon}_r & r_i < r \le \bar{r}_e \\ \varepsilon_r - \varepsilon_r^e & \bar{r}_e < r \le r_e \end{cases} \tag{9}$$

where ε_r is total radial strain within plastic rock mass, $\bar{\varepsilon}_r$ and ε_r^e are the radial strain within the rock mass before the bolts installation in the initial and developed plastic zone, respectively. Reminding that prior to the bolts installation, a plastic displacement in the initial plastic zone, $\bar{r}_e$, and the elastic deformations in the greater plastic zone, r_e, had been developed (Fig. 1b).

To solve differential Eqs. (3) and (4), it is essential to employ a numerical method due to their algebraic complexity. For this purpose, Brown et al. (1983) analytical-numerical method with inclusion of the rockbolt parameters is used to calculate stresses and strains around reinforced circular tunnel. This method is an iterative finite difference solution in which the plastic zone is split into annular rings. The differential equation (3) is rewritten for a ring i.e.

$$\frac{\sigma_{r(j-1)}-\sigma_{r(j)}}{r_{(j-1)}-r_{(j)}}=\frac{\left[\frac{m_a\sigma_c}{2}\left(\sigma_{r(j)}+\sigma_{r(j-1)}\right)+s_a\sigma_c^2\right]^{1/2}}{\frac{r_{(j)}+r_{(j-1)}}{2}}+\frac{T_{(j-1)}-T_{(j)}}{r_{(j-1)}-r_{(j)}}\cdot\frac{r_i}{C_0}\cdot\frac{2}{r_{(j)}+r_{(j-1)}} \tag{10}$$

in which

$$m_a=\frac{m_{(j-1)}+m_{(j)}}{2} \tag{11}$$

$$s_a=\frac{s_{(j-1)}+s_{(j)}}{2} \tag{12}$$

Manipulating Eq. (10) results the second order equation giving $\sigma_{r(j)}$

$$a\cdot\sigma_{r(j)}^2+b\cdot\sigma_{r(j)}+c=0 \tag{13}$$

and solution is

$$\sigma_{r(j)}=\frac{-b-\sqrt{b^2-4ac}}{2a}$$

For $r_i<r\le\bar{r}_e$ zone

$$a=\frac{1}{4K^2}\quad,\quad b=-\frac{K_1-\bar{K}_1}{K}-\frac{\sigma_{r(j-1)}}{2K^2}-2K_2$$

$$c=\sigma_{r(j-1)}\left[\frac{\sigma_{r(j-1)}}{4K^2}+\frac{K_1-\bar{K}_1}{K}-2K_2\right]+\left(K_1-\bar{K}_1\right)^2-s_a\sigma_c^2 \tag{14}$$

where

$$\gamma=d\varepsilon_{r(j)}=\varepsilon_{r(j)}-\varepsilon_{r(j-1)} \tag{15}$$

$$K_1 = \frac{A_b E_s r_i}{C_0\left(r_{(j-1)} - r_{(j)}\right)}\gamma \tag{16}$$

$$\bar{\gamma} = d\bar{\varepsilon}_{r(j)} = \bar{\varepsilon}_{r(j)} - \bar{\varepsilon}_{r(j-1)} \tag{17}$$

$$\bar{K}_1 = \frac{A_b E_s r_i}{C_0\left(r_{(j-1)} - r_{(j)}\right)}\bar{\gamma} \tag{18}$$

and for $\bar{r}_e < r \le r_e$ zone

$$a = \frac{1}{4K^2} \quad , \quad b = -\frac{K_1 - K_1^e}{K} - \frac{\sigma_{r(j-1)}}{2K^2} - 2K_2$$

$$c = \sigma_{r(j-1)}\left[\frac{\sigma_{r(j-1)}}{4K^2} + \frac{K_1 - K_1^e}{K} - 2K_2\right] + \left(K_1 - K_1^e\right)^2 - s_a\sigma_c^2 \tag{19}$$

where

$$\gamma^e = d\varepsilon^e_{r(j)} = \varepsilon^e_{r(j)} - \varepsilon^e_{r(j-1)} \tag{20}$$

$$K_1^e = \frac{A_b E_s r_i}{C_0\left(r_{(j-1)} - r_{(j)}\right)}\gamma^e \tag{21}$$

After finding the distribution of the stress and strain around circular tunnel, the axial force along the bolt (in the ideal condition) can be obtained by Eq. (7).

Modeling of shear displacement between the bolt and rock mass

To find the bolt force in the reality (to be used in Eq. (10)), the relative shear displacement between the bolt and the rock should be calculated. For this purpose, the following new method is proposed. The force applied through the bolt head deforms the tunnel surface beneath the plate, and the bolt elongation is reduced (Fig. 2). It can be said that the reduction of the reinforcement elongation (δ_{rein}) is identical to the deformation of the tunnel surface (Δ_s).

$$\left|\Delta_s\right| = \left|\delta_{rein}\right| \tag{22}$$

In fact, a portion of the force through the bolt head is devoted for the initial bedding in the components of nut and washer on the plate, bedding of the plate on the rock mass, and compressing of the rock mass. Hence, the force in the bolt head is reduced from $T_{\max}$ to T_s . ($T_{\max}$ and T_s are the forces through the bolt head in the ideal and the real conditions, respectively).

From Eq. (22), it can be written

$$\frac{T_s}{K_s} = \frac{T_{rein}}{K_{rein}} \tag{23}$$

where K_{rein} is the shear stiffness of the reinforcing element, and K_s describes the equivalent stiffness of the components of nut and washer and the plate's basement. When a stiff end plate tightened to the bolt head (perfect constraint), it is estimated that $K_s \cong (0.5 - 0.8)K_{rein}$ (For the weak rock mass and high in-situ stress, the lower coefficient is used). This is proven in Appendix A (II). However; when a perfect constraint is not guaranteed, the magnitude of K_s is drastically reduced (Oreste 2008) and becomes a very small value. T_{rein} is the magnitude of bolt head force reduction i.e.

$$T_{rein} = T_{\max} - T_s \tag{24}$$

Combining Eq. (23) and Eq. (24), it can be written

$$T_s = \frac{K_s}{K_s + K_{rein}} T_{\max} \tag{25}$$

From above discussion, it can be assumed that T_{rein} acts as a compression force through the bolt head to reduce the bolt elongation and reduces the bolt force from $T_{\max}$ to T_s.

In the case of the pre-tensioned grouted rockbolts, the computation of the real force applied by the bolt to the tunnel surface may be carried out in two steps as follows:

(1) The computation of the real force due to the pre-tensioned force.

(2) The computation of the real force due to the subsequent load may probably occur after full grouting of the bolt length.

For *Case A*, the real force should be only computed due to the pre-tensioned force. As fictitious compression force acts from the bolt head towards the rock mass, the reduction takes place in two sections of the bolt length i.e. in the free length section (un-grouted section) and in the initially anchored length section as observed in Fig. (3).

$$\delta_{rein} = \delta_{free} + \delta_{anch} \tag{26}$$

where δ_{free} and δ_{anch} are respectively the reduction of the bolt elongation in the free length and anchored length of the bolt obtained by

$$\delta_{free} = \frac{T_{rein}}{K_{free}} \tag{27}$$

$$\delta_{anch} = \frac{T_{rein}}{K_{anch}} \tag{28}$$

in which

$$K_{free} = \frac{E_b.A_b}{L_{free}} \tag{29}$$

$$K_{anch} = \frac{H}{\lambda}\left(\frac{e^{\lambda L_{anch}} + e^{-\lambda L_{anch}}}{e^{\lambda L_{anch}} - e^{-\lambda L_{anch}}}\right) \quad (30)$$

where K_{free} and K_{anch} are the axial stiffness of the free and total anchored length of the bolt for *Case A*, respectively; (See Appendix A (I) for detailed derivation of K_{anch}). L_{free} and L_{anch} are the free and the anchored length of the bolt, and H is a material parameter associates to the shear stiffness between the bolt and the rock mass, and its formulation is available in Appendix A (I). λ is a parameter defined as

$$\lambda = \left(\frac{H}{E_{rein}.A_{rein}}\right)^{0.5} \quad (31)$$

where A_{rein} and E_{rein} are the area section and the elasticity Modulus of the reinforcement, respectively.

Substituting Eqs. (27) and (28) into Eq. (26), and then simplifying gives

$$K_{rein}{}^{A} = \frac{K_{free}.K_{anch}}{K_{free} + K_{anch}} \quad (32)$$

For *Case A*, $T_{\max}$ in Eq. (27) equals to T_{pre}, and superscript A in above equations refers to *Case A*.

Combining Eq. (25) and Eq. (32) gives the real force on the tunnel surface for *Case A* (or for the pre-tensioned force)

$$T_s{}^{A} = \frac{K_s\left(K_{free} + K_{anch}\right)}{K_s K_{free} + K_s K_{anch} + K_{free} K_{anch}} T_{pre} \quad (33)$$

and from Eq. (24)

$$T_{rein}{}^{A} = \eta.T_{pre} \quad (34)$$

$$\eta = \frac{K_{free} K_{anch}}{K_s K_{free} + K_s K_{anch} + K_{free} K_{anch}} \quad (35)$$

Now, from Eq. (24), distribution of force can be obtained. As the initial anchored length is assumed to be located beyond the plastic zone, the distribution of force in that length of bolt is not here studied.

For *Case B*, the bolt is tensioned by both the pre-tensioned force (Fig. 4a) and the movement of rock mass towards tunnel (Fig. 4b). The real force applied on the tunnel surface by the pre-tensioned force can be calculated by a similar formulation of *Case A*. The real force applied on the tunnel surface by the movement of rock mass can be obtained by

$$T_s^{(2)} = \frac{K_s}{K_s + K_{rein}^{(2)}} T_{\max}^{(2)} \tag{36}$$

where $K_{rein}^{(2)}$ is the axial stiffness of free length of the bolt where it is grouted after pre-tensioning calculated by

$$K_{rein}^{(2)} = \frac{H}{\lambda}\left(\frac{e^{\lambda L} + e^{-\lambda L}}{e^{\lambda L} - e^{-\lambda L}}\right) \tag{37}$$

where L is the length of the bolt located in the plastic zone, and $T_{\max}^{(2)}$ is the maximum force of the bolt in the second step. It can be obtained by subtracting the pre-tensioned force from the total maximum force in the ideal condition. (Superscripts (1) and (2) refer to the first and second steps of the bolt tensioning, respectively).

The total real force on tunnel surface may be computed by

$$T_s^{(1)} + T_s^{(2)} = \frac{K_s\left(K_{free} + K_{anch}\right)}{K_s K_{free} + K_s K_{anch} + K_{free} K_{anch}} T_{pre} + \frac{K_s}{K_s + K_{rein}^{(2)}} T_{\max}^{(2)} \tag{38}$$

Considering that Eq. (33) is the extension of Eq. (25), Eq. (38) will be

$$T_s^B = \frac{K_s}{K_s + K_{rein}^{(1)}} T_{pre} + \frac{K_s}{K_s + K_{rein}^{(2)}}\left(T_{\max} - T_{pre}\right) \tag{39}$$

where T_s^B is the real force on the tunnel surface for *Case B*.

The distribution of real force along the bolt for *Case B* will be obtained by

- For the first step (similar to *Case A*)

$$T^{(1)} = T_{pre} - T_{rein}{}^{(1)} \qquad 0 \le x < L_{free} \tag{40a}$$

- For the second step (coupling behavior of the bolt and the rock mass)

$$T^{(2)} = T_{ideal}{}^{(2)} - \left[-\left(T_{\max}{}^{(2)} - T_s{}^{(2)}\right)\frac{e^{-\lambda L}}{e^{-\lambda L} + e^{\lambda L}} e^{\lambda . x} - \left(T_{\max}{}^{(2)} - T_s{}^{(2)}\right)\frac{e^{\lambda L}}{e^{-\lambda L} + e^{\lambda L}} e^{-\lambda . x} \right] \qquad 0 \le x < L_{free} \tag{40b}$$

where x denotes the arbitrary section of bolt length i.e. $x = 0$ at $r = r_i$ and $x = L$ at $r = r_e$.

Therefore, summing of Equations (40a) and (40b), and after some manipulations, the distribution of axial force along the bolt for *Case B* can be calculated as

$$T = T_{ideal} - \eta . T_{pre} - \left[-\left(T_{\max} - T_{pre}\right)\left(1 - \beta\right)\left(\frac{e^{-\lambda L}}{e^{-\lambda L} + e^{\lambda L}}\right)\left(e^{\lambda . x} + e^{2\lambda L} e^{-\lambda x}\right)\right] \tag{41}$$

in which

$$\beta = \frac{K_s}{K_s + K_{rein}{}^{(2)}} \tag{42}$$

Calculation of tunnel convergence considering the real force

As the obtained equilibrium equation is solved by the finite difference method (i.e. Eq. (10)), Eq. (41) should be written as the iterative way. For ring $r_{(j)}$

$$T_{(j)} = T_{ideal(j)} - \eta.T_{pre} - \left[-\left(T_{\max} - T_{pre}\right)\left(1-\beta\right)\left(\frac{e^{-\lambda L}}{e^{-\lambda L}+e^{\lambda L}}\right)\left(e^{\lambda.\left(r_{(j)}-r_i\right)} + e^{2\lambda L} e^{-\lambda\left(r_{(j)}-r_i\right)}\right)\right] \tag{43}$$

Substituting Eq. (43) into Eq. (10) gives

$$\frac{\sigma_{r(j-1)} - \sigma_{r(j)}}{r_{(j-1)} - r_{(j)}} = \frac{\left[\frac{m_a \sigma_c}{2}\left(\sigma_{r(j)} + \sigma_{r(j-1)}\right) + s_a \sigma_c^2\right]^{1/2}}{\frac{r_{(j)} + r_{(j-1)}}{2}} + \left|\frac{T_{(j-1)} - T_{(j)}}{r_{(j-1)} - r_{(j)}} \cdot \frac{r_i}{C_0} \cdot \frac{2}{r_{(j)} + r_{(j-1)}}\right| \tag{44}$$

The value of $T_{(j-1)} - T_{(j)}$ in the either side of neutral point (the location of maximum force along the bolt) is the opposite to each other; the absolute value is used in Eq. (44)

The similar performing process and defined parameters which were used to solve Eq. (10) are applied to Eq. (44) except that the parameter $K_1 - \overline{K}_1$ (or $K_1 - K_1{}^e$) is replaced by Eq. (45).

$$K_1 = \frac{T_{(j-1)} - T_{(j)}}{r_{(j-1)} - r_{(j)}} \frac{r_i}{C_0} \tag{45}$$

Hence, multipliers of the second order Eq. (13) will change to

$$b = \frac{K_1}{K} - \frac{\sigma_{r(j-1)}}{2K^2} - 2K_2 \qquad\qquad a = \frac{1}{4K^2}$$

$$c = \sigma_{r(j-1)}\left[\frac{\sigma_{r(j-1)}}{4K^2} - \frac{K_1}{K} - 2K_2\right] + K_1{}^2 - s_a \sigma_c^2 \tag{46}$$

Appendix B sets out the stepwise sequence of calculations provided in the section 2.

The consideration of a relative shear displacement results in a rotation of principal stresses. That is, the radial and tangential stresses will not be longer principal stresses as assumed in the ideal derivation of bolt force. However, it is assumed in this paper, the produced shear stress is not so great that the principal stresses direction is greatly changed to eclipse the results. It is a venial assumption at least in some conditions e.g. where the pre-tensioned force value, the bolt's density, or rock mass Young's Modulus is great.

Examples

A computer program was prepared to solve the differential equations developed by the finite difference method.

Example 1. The proposed theoretical solution is applied to the Kielder experimental tunnel to compare the accuracy of its results with the actual performance of bolts. The Kielder Experimental Tunnel was driven through four rock mass types. The tunnel in the mudstone was highly unstable, and required most support. The engineering properties of mudstone are available in Table (1). Eight sections with different support systems were constructed in which extensometers were also installed to monitor movement of the rock mass. One of the sections was left unsupported while two sections included combination of the passive grouted rockbolts and shotcrete. One of the sections is also supported by passive grouted rockbolts only. The geometrical parameters of two systems are available in Table (2).

According to Ward et al. (1976), total short-term movement of tunnel surface in the unsupported section of mudstone was about $8\ mm$ in which less than $1\ mm$ had occurred before the face reached, and about $6\ mm$ when the face had advanced $2\ m$ beyond this position. If the reinforcement system was installed just in front of the face, it can be expected that tunnel closure was about 1-2 mm prior to bolt installation (assumed value is 1.5 mm in this paper).

Fig. (5) shows the corresponding ground response curves, and Table (3) gives the calculated and the measured deformations data at tunnel surface for the supported and unsupported rock mass (sequence of calculations was performed by the algorithm presented in Appendix B). As observed, the proposed method can almost predict the identical results and agree with the in-situ measurements in a satisfactory way.

A perfect constraint from the end- plate is predicted in the case of using rockbolt together with shotcrete. This is because, a complete planner contact between the bolt head and the tunnel surface is obtained, and the bolts will take higher loads at the tunnel surface in comparison with the condition that not perfect constraint is foreseen.

Example 2. A highway tunnel with 10.7 m in diameter is driven in a fair to good quality limestone at a depth of 122 m below the surface (Brown et al. 1983). The material property data for the rock mass and in-situ stress are available in Brown et al. (1983).

The pre-tensioned grouted rockbolts are installed by $T_{pre-ten} = 17 \ \ ton$ with $C_0 = 1 \ \ m^2$, $L = 3.15 \ \ m$ when the fictitious constrained pressure is $p_{inst} = 16.5 \ \ ton/m^2$ (the other parameters is assumed to be similar to Example 1). If it is assumed a complete constrained is provided by the end plate, the pre-tensioned pressure is greater than the fictitious constrained pressure of tunnel face. Consequently, the circumstance of *Case A* will take place. The output results are shown in Fig. (6) and Table (4). The efficiency of pre-tensioning can now be best assessed and observed. Therefore, the convergence of tunnel by the pre-tensioning of bolts is reduced considerably.

If the pre-tensioned grouted rockbolts are installed by $T_{pre-ten} = 10 \quad ton$, the circumstance of *Case B* will take place. Fig. (6) shows the ground response curve for this case.

A new practical method for the design of the pre-tensioned grouted bolts

Although the proposed model almost predicts the accurate performance of the passive and the pre-tensioned grouted bolts, its formulas are too complicated to be used as a preliminary design tool, and always need a computer program to carry out the computation procedures. Hence, it will be worth introducing a simple method on the basis of new presented approach parameters to be used as a rule of thumb method in practice.

For *Case A*, the bolt and the rock mass interaction behavior is similar to that of the support systems (such as shotcrete or the pre-tensioned un-grouted bolts) rather than to the reinforcement systems. Therefore, Ground Response Curve (GRC) of the un-supported rock mass and Support Characteristic Curve of a pre-tensioned bolt are plotted (solid line for this Case) to obtain the ultimate tunnel convergence. As seen in Fig. (7), the ultimate convergence is equal to that in the installation time.

The pre-tensioned un-grouted bolt characteristic curve can be obtained by the Eq. (47) (Stille et al. 1989)

$$p_i = k_{sys} . \Delta u_i + p_{pre-ten} \tag{47}$$

where k_{sys} is the support system stiffness calculated by (Stille et al. 1989)

$$k_{sys} = \frac{A_b . E_b}{C_0} \frac{1}{L_{free}} \frac{1}{\xi} \tag{48}$$

Eq. (48) is the stiffness of support system which the reinforcement effect is smeared within the zone of its influence. Thus, the stiffness of a single element is calculated by

$$k = \frac{A_b . E_b}{L_{free}} \frac{1}{\xi} = K_{free} \frac{1}{\xi} \tag{49}$$

ξ is a factor describing the local deformations occurring in the anchoring zone (the far boundary), under the end plate and the bolt head (the near boundary). Stille et al. (1989) pointed out that ξ is an empirical factor which can be determined from Hoek and Brown's (1980) published pull-out tests data of a variety of mechanical and chemically anchored rockbolts. However, those data were not guaranteed to give the accurate results, and were strongly recommended to be determined from field tests on the bolts for critical applications.

It seems that it will be worth developing an analytical approach to obtain ξ.

Flexibility of the complex of bolt head component and the initial anchored length lead to decreasing the axial stiffness of single reinforcement. This is because their deformations under the applied force reduce bolt elongation.

On the other hand, according to the proposed method, the axial stiffness of pre-tensioned un-grouted rockbolt can be calculated by

$$\frac{1}{K_b} = \frac{1}{K_{anch}} + \frac{1}{K_{free}} + \frac{1}{K_s} \tag{50}$$

where K_b is total axial stiffness of reinforcement element.

Equating right hand of Eq. (50) with that of Eq. (49), and then simplifying gives

$$\xi = 1 + \frac{K_{free}}{K_{anch}} + \frac{K_{free}}{K_s} \tag{51}$$

For *Case B*, the ultimate tunnel convergence will be at the intersection point of the diagonal line of Support characteristic curve and the Ground Response Curve of the un-supported rock mass (Dashed line in Fig. 7).

However, this solution is not very exact in case the entire length of the bolt is grouted, and the bolt interacts with its surrounding grout and rock mass. In other words, the bolts confine tunnel convergence not only by applying radial pressure to tunnel surface (like the support systems e.g. un-grouted pre-tensioned bolts), but also by improving rock mass strength quality (like the reinforcement systems e.g. the passive grouted rockbolts).

Therefore, to extend this new approach for *Case B*, the pre-tensioned grouted rockbolts behavior is simulated as a combination of both the support and the reinforcement systems. That is, the improved rock mass and the pre-tensioned un-grouted bolts act independently. The ground response curve of reinforced rock mass by the passive grouted rockbolts is calculated and plotted, and then the support characteristic curve of the pre-tensioned un-grouted bolts plotted separately. The intersection point of two curves gives tunnel convergence which is reinforced by pre-tensioned grouted rockbolts.

No end-plate should be considered for the passive grouted rockbolts. This is because the end-plate effect is taken into account in the behavior of un-grouted pre-tensioned bolt. If the end-plate does not exist, then K_s will be zero, and $T_s = 0$. Consequently the distribution of axial stress along the passive grouted bolts without the end-plate is

$$T^{pass} = T_{ideal}{}^{pass} - \left[-T_{\max}{}^{pass} \frac{e^{-\lambda L}}{e^{-\lambda L} + e^{\lambda L}} e^{\lambda . x} - T_{\max}{}^{pass} \frac{e^{\lambda L}}{e^{-\lambda L} + e^{\lambda L}} e^{-\lambda . x} \right] \tag{52}$$

Superscript *pass* refers to the passive grouted bolts.

This new approach is employed to solve Example 2 for *Case B*. The output results are available in Table (5) and Fig. (8). The intersection point of the support characteristic curve and the ground response curve of the reinforced tunnel (by the passive grouted bolts without face-plate) gives the ultimate convergence of tunnel. As observed, this approach predicts almost the identical convergence obtained in Example 2.

The convergence of tunnel supported by un-grouted pre-tensioned rockbolts is almost identical to that of employing the grouted types. In other words, the grouting effect of bolt is not very effective, and can be neglected. However, on the basis of the proposed model concepts and as it can be seen from Fig. (8), when either the pre-tensioned force is not great enough or the stiffness of the pre-tensioned bolt system is small (e.g. the value of ξ is great), the grouting effect can be considerable.

As a practical design tool, if complete constraint is provided for the near end of bolt head, the pre-tensioned fully grouted bolts can be treated as un-grouted types and its grouting effect is only considered as a factor improving safety.

Conclusions

New analytical approach was proposed for the design the pre-tensioned grouted rockbolts in tunnels based on convergence confinement method. The relationship between the value of constrained radial stress at bolt installation time and the value of applied pre-tensioned pressure was focused on in process of modeling. The near and far boundaries conditions of bolt were also analytically modeled because they can affect the performance of pre-tensioned bolts.

Due to the complexity of theoretical approach for design purposes, a simple method on the basis of new given approach was finally introduced.

The practical outcome of this paper is that if the complete constraint is provided for the near end of bolt head, the grouting effect of the pre-tensioned fully grouted bolts on tunnel stability can be neglected. Therefore, they can be designed by the similar approach of un-grouted pre-tensioned bolts. However, if it is not possible to apply sufficient pre-tensioned force to the bolts (the pre-tensioned force is not great enough), if the anchoring system of bolt is not proper e.g. using the expansion shell or weak grout, or if the complete planner contact between the bolt head and the tunnel surface is not predicted, the grouting effect will be considerable and the attention should be taken to grout quality.

Appendix A.

(I) Calculation of the axial stiffness of anchored length and full length of grouted rockbolt

As the pre-tensioned force is applied, the free and the anchored length of the bolt are tensioned. The equilibrium of the axial force in the anchored length is

$$T + dT = T + \tau.\pi.d_b.dx \qquad (53)$$

where T is the force in the anchored length, d_b is diameter of bolt, and τ is the shear stress on reinforcement perimeter which can be obtained by

$$\tau = K_{ini}.v \qquad (54)$$

where v is the relative displacement between the rock mass and the bolt, K_{ini} is the initial shear stiffness between the bolt and the rock mass expressed as (Cai et al. 2004a,b)

$$K_{ini} = \frac{H}{\pi d_{rein}} \tag{55}$$

where H is a material parameter associated to the shear stiffness between the bolt and the rock mass and can be computed by Eq. (56)

$$H = \frac{2\pi G_g G_m}{\left[\ln\left(R / r_b\right) - 1/2\right] G_g + \ln\left(r_g / r_b\right) G_m} \tag{56}$$

where r_b and r_g are radius of the bolt and radius of the grout borehole; G_g and G_m is shear modulus of the grout mortar and the rock mass, respectively; and R is the influence radius of a single rock bolt.

Substituting Eq. (54) into Eq. (53) and then taking derivation gives

$$\frac{d^2T}{dx^2} - \lambda^2 T = 0 \tag{57}$$

in which

$$\frac{dv}{dx} = \frac{T}{E_b . A_b} \tag{58}$$

$$\lambda = \left(\frac{K_{ini} . \pi d_b}{E_b A_b}\right)^{0.5} = \left(\frac{H}{E_b A_b}\right)^{0.5} \tag{59}$$

A_b and E_b are the area section and the elastic modulus of the bolt, respectively.

The solution of above differential equation is

$$T = C_1 e^{\lambda . x} + C_2 e^{-\lambda . x} \tag{60}$$

C_1 and C_2 are constants obtained by the following boundary conditions

At $x = L_{free}$ $T = -T_{rein} = -\left(T_{\max} - T_s\right)$

and at $x = L_{free} + L_{anch}$ $v = 0$

where L_{free} is the free length of the bolt which is not grouted in pre-loading process, L_{anch} is the initially anchored length of the bolt securing the anchoring capacity against pre-loading.

Note that $T_{\max}$ is equal to T_{pre} for *Case A*, (and also for the first step of *Case B*). Because, the maximum force is T_{pre} for this case.

Substituting C_1 and C_2 into Eq. (60) and then calculating v at $x = L_{free}$ gives the magnitude of displacement of the bolt in anchored section i.e.

$$v_{anch} = \frac{\lambda . T_{rein}}{H}\left(\frac{e^{\lambda L_{anch}} - e^{-\lambda L_{anch}}}{e^{\lambda L_{anch}} + e^{-\lambda L_{anch}}}\right) \tag{61}$$

therefore

$$K_{anch} = \frac{H}{\lambda}\left(\frac{e^{\lambda L_{anch}} + e^{-\lambda L_{anch}}}{e^{\lambda L_{anch}} - e^{-\lambda L_{anch}}}\right) \tag{62}$$

K_{anch} is the axial stiffness of bolt in the anchored section.

Performing the same process for the second step of *Case B* with the following boundary condition

At $\quad x = 0 \quad T = -T_{rein}^{(2)} = -\left(T_{\max} - T_{pre}\right) - T_s^{(2)}$

and at $\quad x = L \quad v = 0$

gives

$$K_{rein}^{(2)} = \frac{H}{\lambda}\left(\frac{e^{\lambda L} + e^{-\lambda L}}{e^{\lambda L} - e^{-\lambda L}}\right) \tag{63}$$

where $T_{\max}$ is the force on the bolt head in the ideal connection between the bolt and the rock mass, and $T_s^{(2)}$ is the force on the bolt head applied on the tunnel surface in real condition. Superscript (2) refers to the second step of the bolt tensioning which is due to rock mass movement towards tunnel.

(II) Estimation of K_s

From the analysis of the in situ measurements and the results of numerous bi-dimensional numerical calculation in the performed parametric study, Oreste (2008) presented the axial force along the passive grouted bolts, with a certain approximation, by a simple two-line graphic (Fig. 9). When a perfect constraint on the bolt head is predicted, the maximum value of bolt force is at the distance of about $L/6$ from the tunnel wall while the value in the bolt head (T_s) is $2/3$ of the maximum force along the bolt i.e.

$$T_s = \frac{2}{3} T'_{\max} \tag{64}$$

As the distribution of axial force in the "pick up length" is exponential, it can be written $T_s = (0.35 - 0.5) T_{\max}$ (Ranjbarnia 2014). Therefore

$$K_s = (0.5 - 0.8) K_{rein} \tag{65}$$

Evaluation of the results of theoretical approaches carried out for the modelling of passive grouted bolts (Stille et al. 1989; Oreste and Peila 1996; Li and Stillborg 1999, Cai et al. 2004a) and in-situ measurements (Ward et al. 1976) shows the suitability of Eq. (65).

K_{rein} in Eq. (65) is obtained by Eq. (42). This is because; it gives the reinforcement stiffness for the second step of loading which is identical to the loading process of the passive grouted bolts.

Appendix B. Ground response curve calculation for reinforced tunnel

Input data.

σ_c : un- axial compressive strength of intact rock pieces.

m , s : material constants for original rock mass.

E_m , ν : Young’s modulus and Poisson's ratio of original rock mass.

G_g : shear modulus grout.

m_r , s_r : material constants for broken rock mass.

f , h : gradients of $-\varepsilon_3^p$ vs. ε_1^p lines in the residual and the strain softening stages, respectively.

μ : constant defining strain at which residual strength is reached.

p_0 : in situ hydrostatic stress.

r_i : tunnel radius.

d_b : the bolt diameter.

d_g : the hole diameter.

A_b : cross section area of each bolt.

E_s : Young’s modulus of bolt.

C_0 : bolt’s spacing.

$T_{pre-ten}$: pre-tensioning force.

L_{anch} : initial anchored length.

L : total bolt length.

R : the influence limit of each bolt usually is $10d_g$

Preliminary Calculations

$$1)\ M=\frac{1}{2}\left[\left(\frac{m}{4}\right)^{2}+m\frac{p_0}{\sigma_c}+s\right]^{1/2}-\frac{m}{8}$$

$$2)\, G_m=\frac{E_m}{2(1+\upsilon)}$$

$$3)\ H=\frac{2\pi G_g G_m}{\left[\ln\left(R/r_b\right)-1/2\right]G_g+\ln\left(r_g/r_b\right)G_m}$$

$$4)\ \lambda=\left(\frac{H}{E_s.A_b}\right)^{0.5}$$

$$5)\ p_{pre-ten}=T_{pre-ten}/\left(C_0\right)$$

$$6)\ \varepsilon_{pre-ten}=T_{pre-ten}/\left(A_b.E_s\right)$$

$$7)\ L_{free}=L-L_{anch}$$

$$8)\ K_{rein}=\frac{H}{\lambda}\left(\frac{e^{\lambda L}+e^{-\lambda L}}{e^{\lambda L}-e^{-\lambda L}}\right)$$

$$9)\ K_s=\chi.K_{rein} \qquad 0.5<\chi<0.8$$

$$10)\ K_{anch}=\frac{H}{\lambda}\left(\frac{e^{\lambda L_{anch}}+e^{-\lambda L_{anch}}}{e^{\lambda L_{anch}}-e^{-\lambda L_{anch}}}\right)$$

$$11)\ K_{free}=\frac{E_b.A_b}{L_{free}}$$

$$12)\, K_{rein}^{(1)}=\frac{K_{free}.K_{anch}}{K_{free}+K_{anch}}$$

$$13)\ K_{rein}^{(2)}=\frac{H}{\lambda}\left(\frac{e^{\lambda L}+e^{-\lambda L}}{e^{\lambda L}-e^{-\lambda L}}\right)$$

14) $\alpha = \dfrac{K_s}{K_s + K_{rein}{}^{(1)}}$

15) $\beta = \dfrac{K_s}{K_s + K_{rein}{}^{(2)}}$

16) $\eta = \dfrac{K_{free} K_{anch}}{K_s K_{free} + K_s K_{anch} + K_{free} K_{anch}}$

Calculations for the first ring

1) $r_{(1)} = r_e$

2) $\varepsilon_{\theta(1)} = \varepsilon_{\theta(e)} = M\sigma_c / 2G$

3) $\varepsilon_{r(1)} = \varepsilon_{r(e)} = -M\sigma_c / 2G$

4) $\sigma_{r(1)} = \sigma_{re} = p_0 - M.\sigma_c$

5) $\sigma_{\theta(1)} = \sigma_{\theta e} = p_0 + M.\sigma_c$

6) $m_{(1)} = m$

7) $s_{(1)} = s$

8) $\omega_{(1)} = 0$

9) $\zeta_1 = r_{(1)} / r_e = 1$

Sequence of calculations for each ring

1) $d\varepsilon_\theta = 0.005\varepsilon_{\theta(1)}$

2) $\varepsilon_{\theta(j)} = \varepsilon_{\theta(j-1)} + d\varepsilon_\theta$

3) If $\varepsilon_{\theta(j)} \le \mu.\varepsilon_{\theta(1)}$ then $\varepsilon_{r(j)} = \varepsilon_{r(j-1)} - hd\varepsilon_\theta$ otherwise $\varepsilon_{r(j)} = \varepsilon_{r(j-1)} - fd\varepsilon_\theta$

4) $\kappa = \dfrac{2\varepsilon_{\theta(j-1)} - \varepsilon_{r(j-1)} - \varepsilon_{r(j)}}{2\varepsilon_{\theta(j)} - \varepsilon_{r(j-1)} - \varepsilon_{r(j)}}$

5) $\zeta_{(j)} = \kappa.\zeta_{(j-1)}$

6) $\lambda_{(j)} = r_{(j)} / r_e \quad \lambda_{(j-1)} = r_{(j-1)} / r_e$

7) If $\varepsilon_{\theta(j)} \le \mu\varepsilon_{\theta(1)}$ then $m_{(j)} = m + (m_r - m)\dfrac{\varepsilon_{\theta(j)} - \varepsilon_{\theta(e)}}{(\mu - 1)\varepsilon_{\theta(e)}}$ otherwise $m_{(j)} = m_r$

8) If $\varepsilon_{\theta(j)} \le \mu\varepsilon_{\theta(1)}$ then $s_{(j)} = s + (s_r - s)\dfrac{\varepsilon_{\theta(j)} - \varepsilon_{\theta(e)}}{(\mu - 1)\varepsilon_{\theta(e)}}$ otherwise $s_{(j)} = s_r$

9) $m_a = \dfrac{1}{2}\left(m_{(j-1)} + m_{(j)}\right)$

10) $s_a = \dfrac{1}{2}\left(s_{(j-1)} + s_{(j)}\right)$

11) $K_2 = \dfrac{m_a \sigma_c}{4}$

12) $K = \dfrac{\lambda_{(j-1)} - \lambda_{(j)}}{\lambda_{(j)} + \lambda_{(j-1)}}$

13) If $p_{pre-ten} \ge p_{inst}$, then go to step 14, otherwise go to step 18

14) $a = \dfrac{1}{4K^2}$

15) $b = -\dfrac{\sigma_{r(j-1)}}{2K^2} - 2K_2$

16) $c = \sigma_{r(j-1)}\left[\dfrac{\sigma_{r(j-1)}}{4K^2} - 2K_2\right] - s_a \sigma_c^2$

17) Now, go to step 26

18) If $\sigma_{r(j-1)} > p_{inst}$ and then $\omega_{(j)} = 0$, other wise $\omega_{(j)} = \omega_{(j-1)} + 1$

19) $\gamma = d\varepsilon_{r(j)} = \varepsilon_{r(j)} - \varepsilon_{r(j-1)}$

20) $K_1 = \dfrac{A_b E_s r_i}{C_0\left(r_{(j-1)} - r_{(j)}\right)}\gamma$

21) $\bar{\gamma} = d\bar{\varepsilon}_{r(j)} = \bar{\varepsilon}_{r(j-\omega_j)} - \bar{\varepsilon}_{r(j-1-\omega_j)}$ $\quad r_i \le r < \bar{r}_e$

$\gamma^e = d\varepsilon^e_{r(j)} = \varepsilon^e_{r(j)} - \varepsilon^e_{r(j-1)}$ $\quad \bar{r}_e \le r \le r_e$

22) $\bar{K}_1 = \dfrac{A_b E_s r_i}{C_0\left(r_{(j-1)} - r_{(j)}\right)}\bar{\gamma}$ $r_i \le r < \bar{r}_e$

$\bar{r}_e \le r \le r_e$ $\quad K_1^e = \dfrac{A_b E_s r_i}{C_0\left(r_{(j-1)} - r_{(j)}\right)}\gamma^e$

23) $a = \dfrac{1}{4K^2}$

24) $b = -\dfrac{K_1 - \bar{K}_1}{K} - \dfrac{\sigma_{r(j-1)}}{2K^2} - 2K_2$ $r_i \le r < \bar{r}_e$

$\bar{r}_e \le r \le r_e$ $\quad b = -\dfrac{K_1 - K_1^e}{K} - \dfrac{\sigma_{r(j-1)}}{2K^2} - 2K_2$

25) $c = \sigma_{r(j-1)}\left[\dfrac{\sigma_{r(j-1)}}{4K^2} + \dfrac{K_1 - \bar{K}_1}{K} - 2K_2\right] + \left(K_1 - \bar{K}_1\right)^2 - s_a\sigma_c^2$

$r_i \le r < \bar{r}_e$

$c = \sigma_{r(j-1)}\left[\dfrac{\sigma_{r(j-1)}}{4K^2} + \dfrac{K_1 - K_1^e}{K} - 2K_2\right] + \left(K_1 - K_1^e\right)^2 - s_a\sigma_c^2$

$\bar{r}_e \le r \le r_e$

26) $\Delta = b^2 - 4a.c$

27) $\sigma_{r(j)} = \dfrac{-b - \sqrt{\Delta}}{2a}$

28) If $\sigma_{r(j)} > p_i$, then increment j by 1 and repeat the calculation sequence for next ring.

29) If $\sigma_{r(j)} \approx p_i$, then $r_{(j)} = r_i$; $r_e = r_{(j)} / \lambda_{(j)}$.

Note: p_i should not be decreased from $p_{pre-ten}$.

30) If $\sigma_{r(j)} \approx p_{inst}$, then $\bar{r}_e = r_e$

31) The radii of all the rings may now be calculated, using $r_{(j)} = \lambda_{(j)}.r_e$

32) The displacement values of rings may be determined from the previously computed values of $u_j = -\varepsilon_{\theta(j)}.r_{(j)}$

33) $T_{ideal(j)} = A_b.E_s.\left(\varepsilon_{r(j)} - \varepsilon_{r(j-\omega_j)} + \varepsilon_{pre-ten}\right)$

34) If $\sigma_{r(j)} \approx \min\{p_{inst}, p_{pre-ten}\}$, then $T_{ideal(j)} = T_{\max}$

35) After calculating $T_{\max}$, the steps 1 to 12 are repeated.

36) $T_s = (1-\eta).T_{pre}$

37) $p'_{pre-ten} = T_s / C_0$

38) If $p'_{pre-ten} \geq p_{inst}$, then $T_{(j)} = (1-\eta).T_{pre}$ and go to step 39, otherwise go to step 40

39) the steps 14 to 16 and steps 26 to 29 are repeated except that $p_{inst} < p_i < p_0$. Go to step 46.

40) $T_{(j)} = T_{ideal(j)} - \eta.T_{pre} - \left[-\left(T_{\max} - T_{pre}\right)(1-\beta)\left(\dfrac{e^{-\lambda L}}{e^{-\lambda L} + e^{\lambda L}}\right)\left(e^{\lambda.\left(r_{(j)} - r_i\right)} + e^{2\lambda L} e^{-\lambda\left(r_{(j)} - r_i\right)}\right)\right]$

41) $K_1 = \dfrac{T_{(j-1)} - T_{(j)}}{r_{(j-1)} - r_{(j)}} \dfrac{r_i}{C_0}$

42) $a = \dfrac{1}{4K^2}$

43) $b = \dfrac{K_1}{K} - \dfrac{\sigma_{r(j-1)}}{2K^2} - 2K_2$

44). $c = \sigma_{r(j-1)}\left[\dfrac{\sigma_{r(j-1)}}{4K^2} - \dfrac{K_1}{K} - 2K_2\right] + K_1{}^2 - s_a \sigma_c^2$

45) Steps 26 to 29 are repeated except that $p'_{pre-ten} < p_i < p_0$.

46) The radii of all the rings may now be calculated, using $r_{(j)} = \lambda_{(j)}.r_e$

47) The displacement values of rings may be determined from the previously computed values of $u_j = -\varepsilon_{\theta(j)}.r_{(j)}$.

References

Aydan, Ö. (1989). "The Stabilisation of Rock Engineering Structures by Rockbolts." Ph. D. thesis, Queens's Univ., Kingston, Ontario.

Bischoff, J.A., Smart, J.D. (1975). "A method of computing a rock reinforcement system which is structurally equivalent to an internal support system." *Proc. of 16th Symp. on Rock Mechanics,* Univ. of Minnesota, 179-184.

Bobet, A. (2006). "A simple method for analysis of point anchored rockbolts in circular tunnels in elastic ground." *Rock Mech. Rock Eng.*, 39, 315- 338.

Bobet, A., Einstein, E. (2011). "Tunnel reinforcement with rockbolts." *Tunnel. Underground Space Tech.,* 26, 100-123.

Brown, E.T., Bray, J.W., Ladanyi, B., and Hoek, E. (1983). "Ground response curves for rock tunnels." *J. of Geotech. Eng.*, 109, 15- 39.

Cai, Y., Esaki, T., and Jiang, Y. (2004a). “An analytical model to predict axial load in grouted rock bolt for soft rock tunneling.” *Tunnel. Underground Space Tech.*, 19, 607- 618.

Cai, Y., Jiang, Y.J., and Esaki, T. (2004b). “A rock bolt and rock mass interaction model.” *Int. J. of Rock Mech. Mining Sci.*, 41, 1055-1067.

Carranza-Torres, C. (2009). “Analytical and Numerical Study of the Mechanics of Rockbolt Reinforcement around Tunnels in Rock Masses.” *Rock Mech. Rock Eng.*, 42, 175- 228.

Fahimifar, A., Soroush, H. (2005). “A theoretical approach for analysis of the interaction between grouted rockbolts and rock masses.” *Tunnel. Underground Space Tech.*, 20, 333-343.

Fahimifar, A., Ranjbarnia, M. (2009). “Analytical approach for the design of active grouted rockbolts in tunnel stability based on convergence-confinement method.” *Tunnel. Underground Space Tech.*, 24, 363-375.

Freeman, T.J. (1978). “The behavior of fully-bonded rock bolts in the Kielder experimental tunnel.” *Tunnels Tunn*, 37–40.

Grasso, P.G., Mahtab, A., and Pelizza, S. (1989). “Riqualificazione della massa roccoisa: un criterio per la atabilizzaazione della gallerie.” *Gallerie e Grandi Opere Sotterranee*, 29, 35- 41.

Guan, Zh., Jiang, Y., Tanabasi, Y., and Huang, H. (2007). “Reinforcement mechanics of passive bolts in conventional tunneling.” *Int. J. of Rock Mech. Mining Sci.,* 44, 625-636.

Hoek, E., Brown, E.T. (1980). “Underground Excavations in Rock.” The Institution of Mining and Metallurgy, London.

Huang, Z., Broch, E., and Lu, M. (2002). “Cavern roof stability- mechanism of arching and stabilization by rockbolting.” *Tunnel. Underground Space Tech.*, 17, 249-261.

Indraratna, B., Kaiser, P.K. (1990a). “Design of grouted rock bolts based on the convergence control method.” *Int. J. Rock Mech. Mining Sci and GeoMech.*, 27, 269-281.

Indraratna, B., Kaiser, P.K. (1990b). “Analytical model for the design of grouted rock bolts.” *Int. J. Numer. Anal. Meth. Geomech.*, 14, 227- 251.

Li, C., Stillborg, B. (1999). “Analytical models for rock bolts.” *Int. J. of Rock Mech. Mining Sci.*, 36, 1013- 1029.

Oreste P.P., Peila, D. (1996). “Radial passive rockbolting in tunneling design with a new convergence-confinement model.” *Int. J. Rock Mech. Mining Sci and GeoMech.,* 33, 443- 454.

Osgoui, R.R., Oreste, P. (2010). “Elasto-plastic analytical model for the design of grouted bolts in a Hoek–Brown medium.” *Int. J. Numer. Anal. Meth. Geomech.*, 34, 1651–1686.

Oreste, P.P. (2008). “Distinct analysis of fully grouted bolts around a circular tunnel considering the congruence of displacements between the bar and the rock.” *Int. J. of Rock Mech. Mining Sci.*, 45, 1052–1067.

Peila, D., Oreste P.P. (1995). “Axisymmetric analysis of ground reinforcing in tunneling design.” *Comput. Geomach.*, 17, 253- 274.

Ranjbarnia, M., (2014). “Theoretical analysis of pre-tensioned grouted rockbolts behavior in tunnels considering the interaction of bolt, grout, and rock mass”, *PhD thesis*, Department Civil and Environmental Engineering, Amirkabir University of Technology, Tehran. Iran

Stille, H., Holmberg, M., and Nord G. (1989). “Support of Weak Rock with Grouted Bolts and Shotcrete.” *Int. J. of Rock Mech. Mining Sci. and Geomech*. 26, 99-l 1

Ward, W.H., Coats, D.J., and Tedd, P. (1976). “Performance of support systems in the Four Fathom Mudstone.” *Proc. of Tunnelling 76*, London, 329-340.

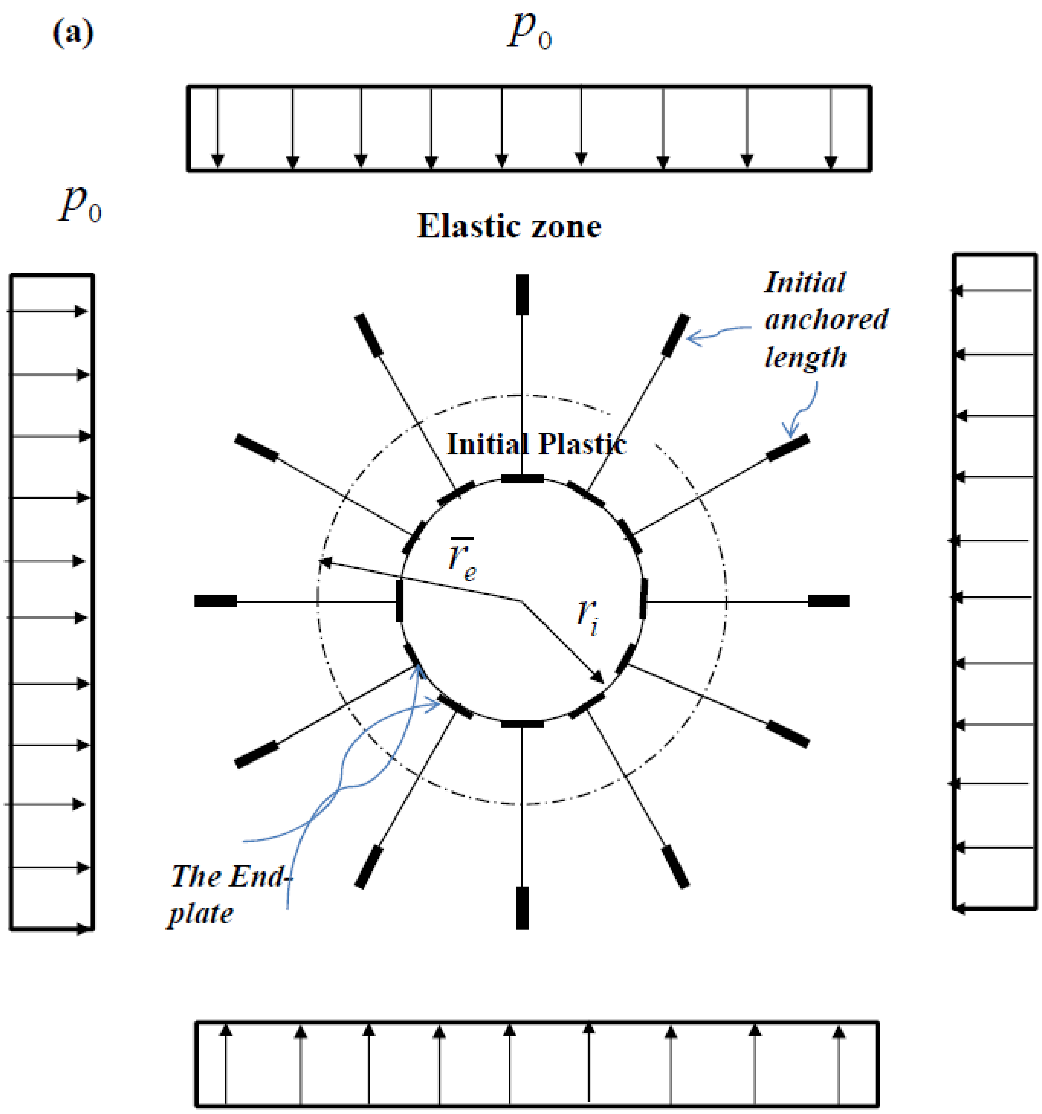

Figure 1. Circular tunnel reinforced by systematic pre-tensioned grouted bolts (a) the plastic radius at the bolt installation time (b) Increasing tunnel plastic radius

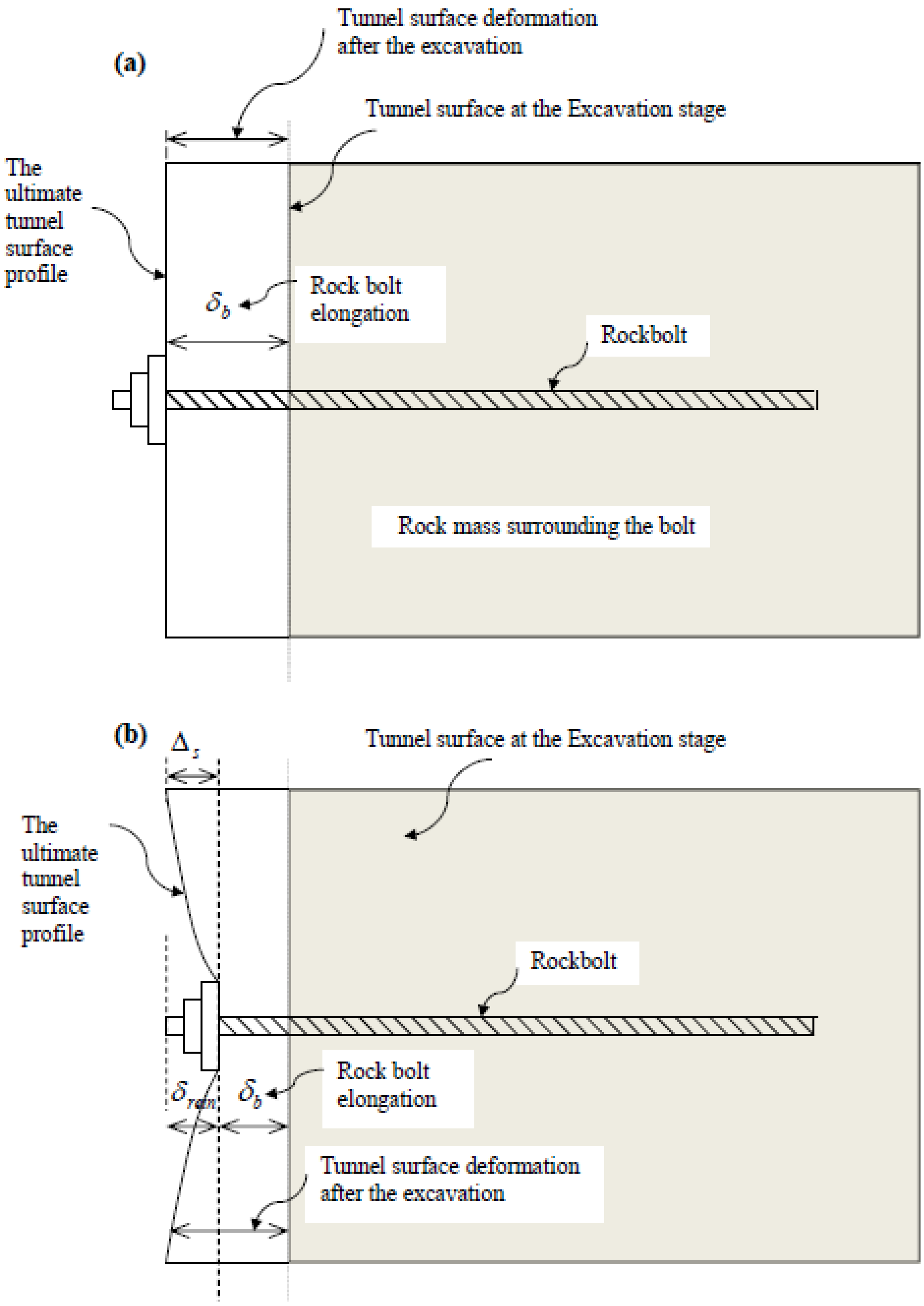

Figure 2. Rock mass and bolt interaction at tunnel surface in (a) ideal connection and (b) real connection between the bolt and rock mass

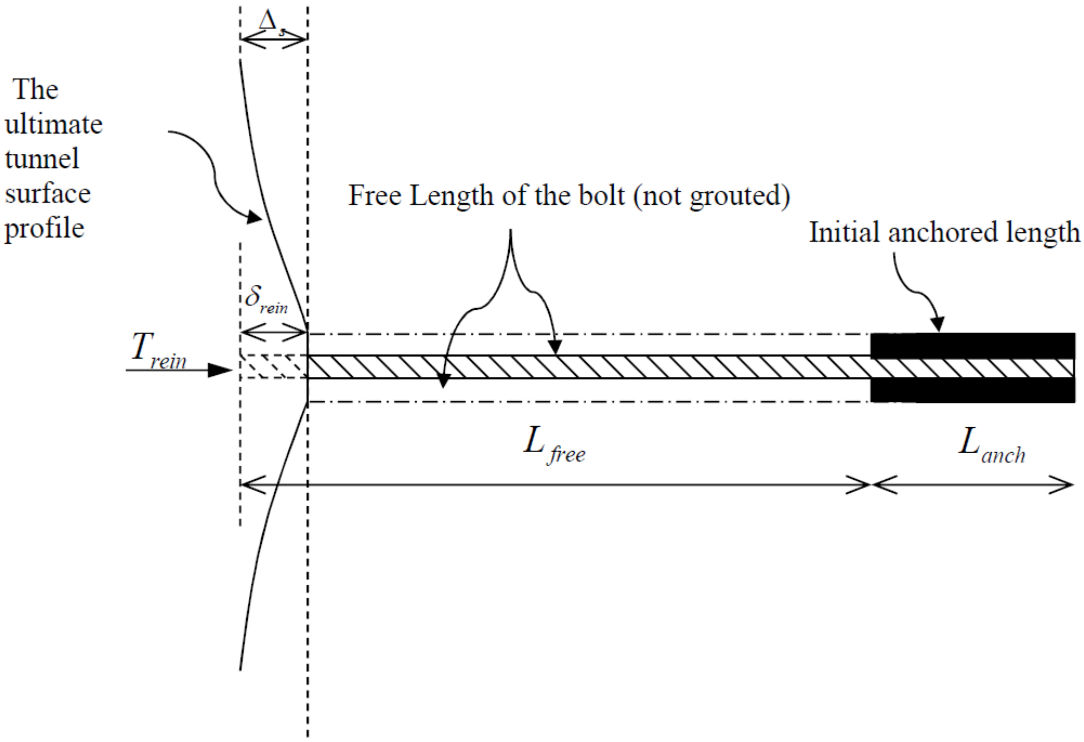

Figure 3. Total reduction of bolt elongation

(a)

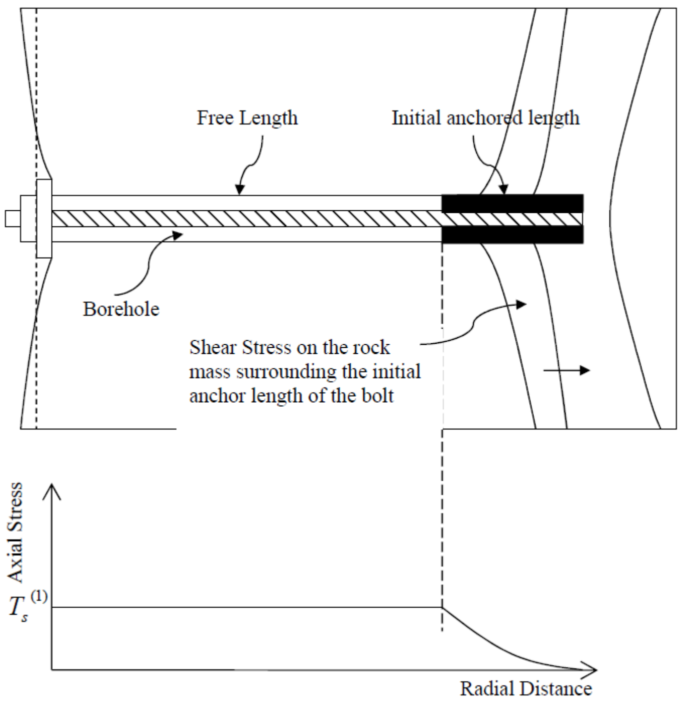
Free Length
Initial anchored length
Borehole
Shear Stress on the rock mass surrounding the initial anchor length of the bolt
Axial Stress
$T_s^{(1)}$
Radial Distance

817

(b)

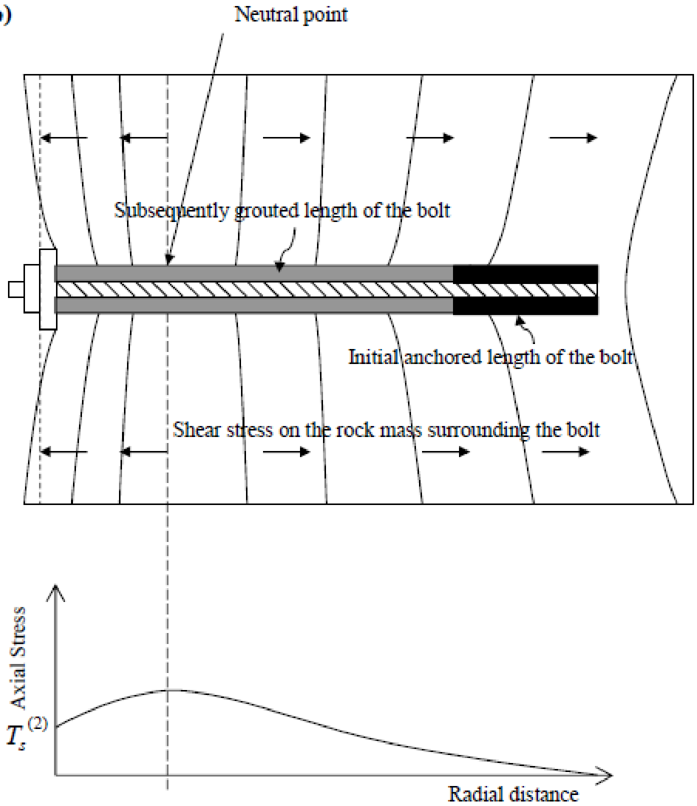
Neutral point
Subsequently grouted length of the bolt
Initial anchored length of the bolt
Shear stress on the rock mass surrounding the bolt
Axial Stress
$T_s^{(2)}$
Radial distance

818

Figure 4. Interaction of bolt with its surrounding rock mass for *Case B*. Loading mechanism of the bolt (a) for the first step (b) for the second step

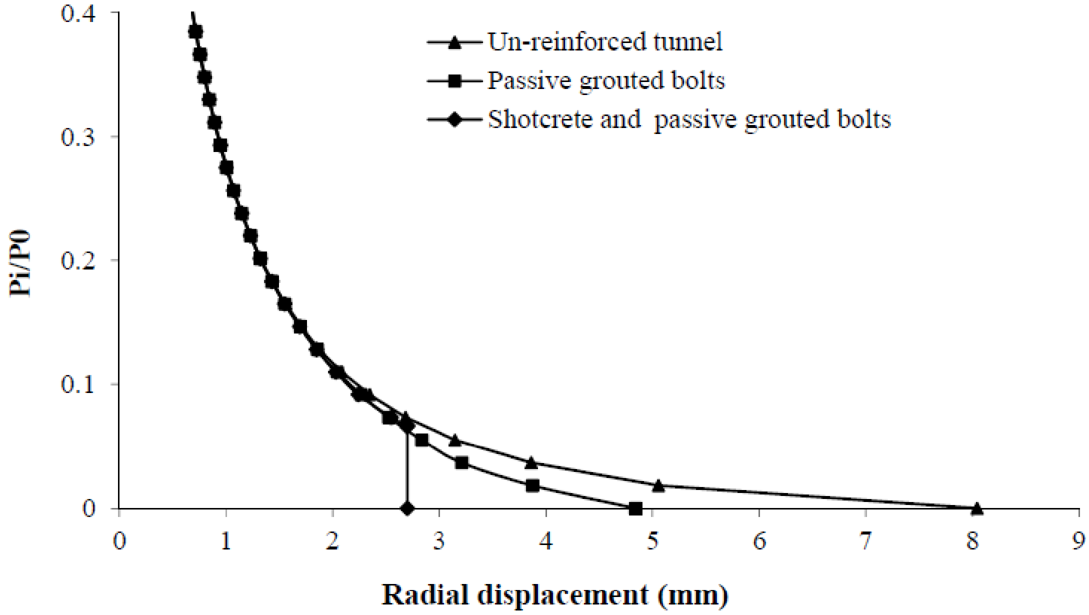

Figure 5. Ground response curves for the rock mass around Kielder Experimental Tunnel (Example 1) in the rockbolted and rockbolt with shotcreted section

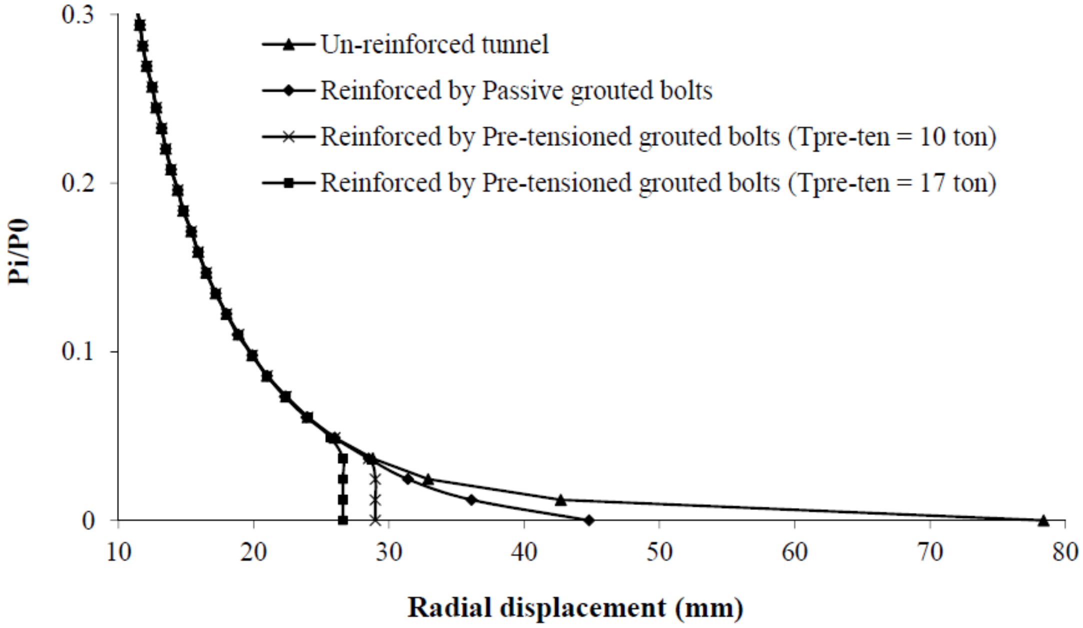

Figure 6. Ground response curve for the rock mass around tunnel in Examples 2 for *Case A* and *Case B*

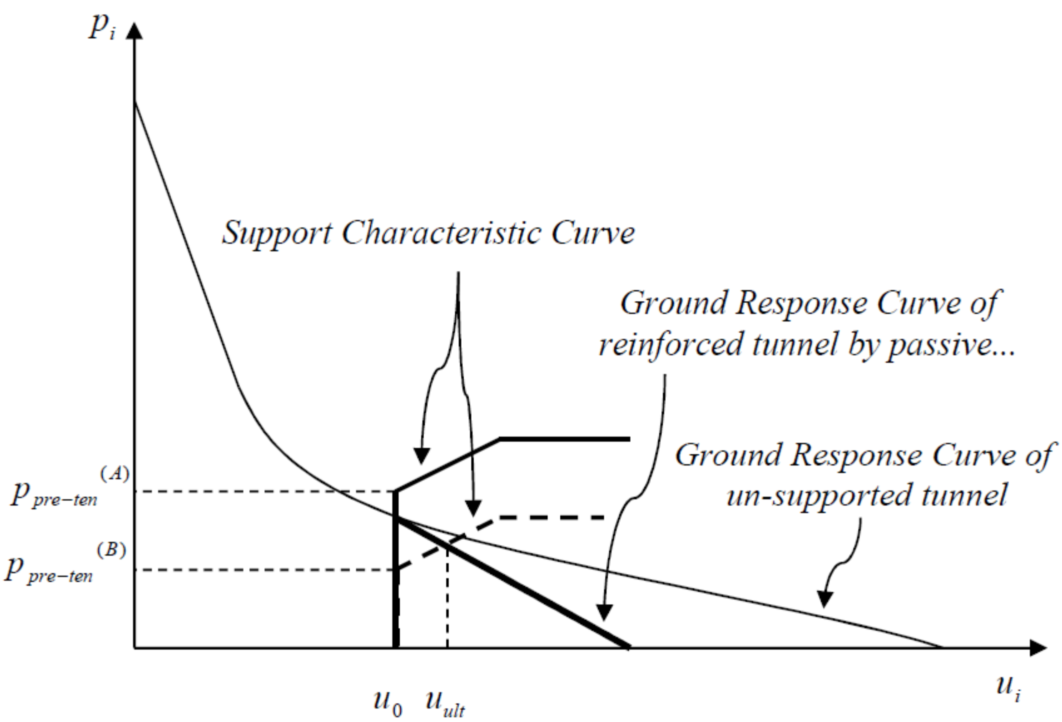

Figure7. Un-grouted pre-tensioned characteristic curve (solid line for *Case A*

condition and dashed line for *Case B* condition) and ground response curves of un-supported tunnel and reinforced by passive grouted bolts

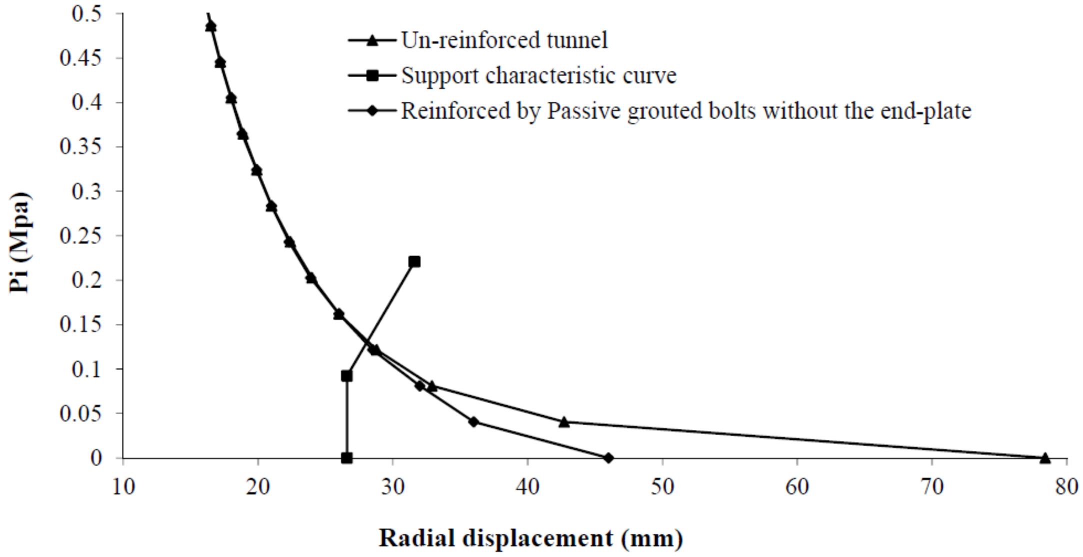

Figure 8. Un- grouted pre-tensioned characteristic curve and the ground response curves of tunnel for un-reinforced and reinforced by passive grouted bolts (Example 2 by simple practical method)

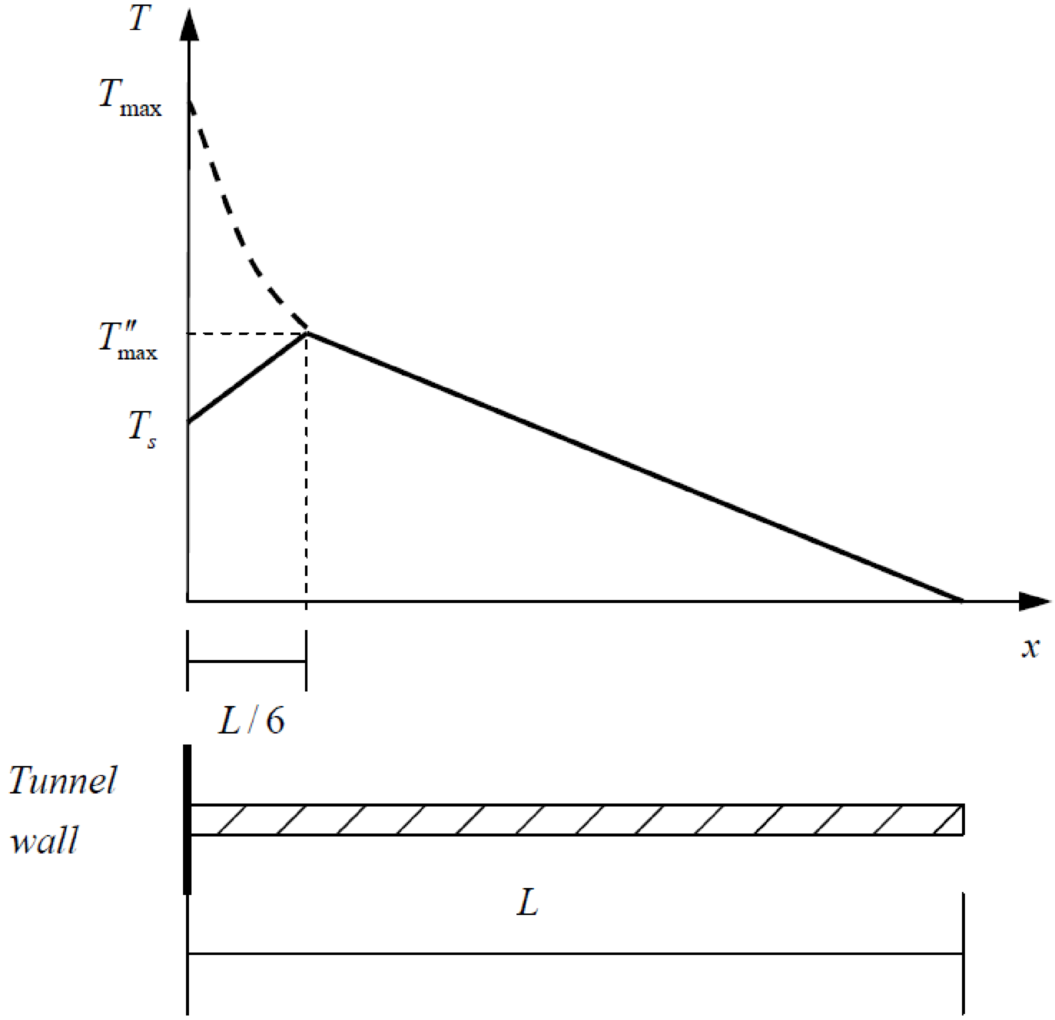

Figure 9. Simplified graphic of force along the bolt (two solid line by Oreste (2008) and dashed curve by Ranjbarnia (2014))

Table 1. Mechanical properties of mudstone in the Kielder Experimental Tunnel (data from Freeman 1978; Hoek and Brown 1980)

Parameter	Value
Axial compressive strength σ_c (MPa)	37
Tunnel radius, r_i (m)	1.65
In-situ stress, p_0 (MPa)	2.56
Deformation modulus, E_m (MPa)	5000
Poisson's ratio, ν	0.25
Peak Strength parameter, m_p	0.1
Peak Strength parameter, s_p	0.00008
Residual Strength parameter, m_r	0.05
Residual Strength parameter, s_r	0.00001
Dilation angle (degree), ψ	10
Strain softening parameters*, gradients of $-\varepsilon_3^p$ vs. ε_1^p lines in the residual stage, f	1.1
Strain softening parameters*, gradients of $-\varepsilon_3^p$ vs. ε_1^p lines in the softening stage, h	1.2
Strain softening parameters*, constant defining strain at which residual strength is reached, μ	7.5

*these parameters were computed by the authors from the value of dilation angle

Table 2. Geometrical parameters of passive grouted rockbolts and shotcrete in the Kielder Experimental Tunnel (data from Ward et al. 1976; Freeman 1978; Hoek and Brown 1980)

Parameter	**Value**
Rockbolt Length, L (m) *	1.8
Initial anchored length, L_{anch} (m)	0.5
Young's modulus of rockbolt, E_s (GPa)	210
Bolt diameter, d_b (mm)	20
Borehole diameter, d_g (mm) **	60
Distance between rockbolt, $S_l \times S_c$ $(m \times m)$	0.9*0.9
Early age Young's modulus of shotcrete, E_{shot} (GPa)	2
Shotcrete thickness, (mm)	140
Bolt head stiffness, K_s (MN) ***	320
Shotcrete pressure on the tunnel surface (MPa) ****	0.17

* According to Hoek and Brown (1980) study, this value was smaller than what was required. Authors of this paper used the required value.

** assumed typical value

***calculated by the authors for the shotcreted section of tunnel where perfect constrained was predicted for the end plate of bolt.

**** calculated by the authors from the classic formula presented by Hoek and Brown (1980). Shotcrete layer radial deformation was 1.5 mm.

Table 3. Calculated and measured deformations (data from Stille et al. 1989) at the rock surface for reinforced and un-reinforced rock mass

Parameter	**Measured** (mm)	**Calculated*** (mm)
Un-reinforced tunnel	8	8.05
Passive grouted bolt section	4-5	4.84
Passive grouted bolt and Shotcrete section	2-3	2.7

*By authors

Table 4. The output results of Example 2

Example		Ultimate convergence (mm)	Plastic radius (mm)
Un-reinforced tunnel		78.4	12.27
Reinforced tunnel	by the passive bolts	44.8	9.37
	by the pre-tensioned bolts (Case A)	26.6	8.1
	by the pre-tensioned bolts (Case B)	29.8	8.42

Table 5. The input and output data of Example 2 calculated by simple practical method

Parameter	Value
σ_{r_0-pre} (Mpa)*	0.0924
ξ	1.2
k_{sys} (MN/m^3)	25.7
u_1 (mm)	26.6
u_{ult} (mm)	28.5

*Calculated by $p_{pre-ten} = T_s / C_0$ where T_s is obtained by Eq. (33)